Broadband Silver Ribbon-Embedded Graphene and h-BN Optical Modulator With High Modulation Depth and Extinction Ratio and Low Switching Voltage

Hossein Karimkhani and Hamid Vahed

***Abstract*—Herein, we theoretically demonstrate a broadband hybrid plasmonic electro-absorption optical modulator with integrated silver nanoribbons. We have examined two structures. The first one includes two layers of graphene and two layers of hexagonal boron nitride (h-BN). Silver nanoribbons are placed on the Molybdenum Disulfide (MoS_2) layer. In the second structure, we covered the nanoribbon arrays with extra graphene, MoS_2, and h-BN layers. The effect of the gap between the silver nanoribbons is analyzed for the effective refractive index, modulation depth (MD), Extinction Ratio (ER), Figure of Merit (FoM), and loss. The best results illustrate that the highest amount of the effective refractive index is 5.65, and the highest amount of the loss is 2.2 dB/μm in the chemical potential of 0.65 eV at the wavelength of 1.3 μm. The maximum MD and FoM are 28.37 dB/μm and 62.93 at 1.3 μm, respectively. The calculations show that this electro-absorption modulator has a modulation bandwidth of 411.25 GHz and 27.18 fJ/bit energy consumption. This modulator achieves a high MD, ER, and FoM with a small footprint and low switching voltage. The study demonstrates that the modulator can achieve a high level of modulation depth with low energy consumption and loss.**

***Index Terms*—Optical modulators, graphene, Molybdenum Disulfide, 2D materials, electro absorption.**

I. Introduction

GRAPHENE is a distinctive 2D material with a carbon atomic layer in a hexagonal lattice. Graphene was introduced in 2004 [1], [2]. Graphene possesses remarkable mechanical strength, chemical stability, electro-optical adjustability, variable gate voltage, high light interaction, and high carrier mobility due to its distinctive band structure [3], [4]. Moreover, graphene is a key material in telecommunication optical devices and components, so it is a great candidate for electro-optical modulators. The graphene layer can be easily integrated with optical fibers and circuits. Graphene has increased the MD and the modulation bandwidth due to its high absorption in optical modulators [5], [6]. Graphene is also used in isotropic and anisotropic models in optical structures [4], [5], [7]. Anisotropic graphene can support TE and TM modes [8]. The main method for controlling the conductivity of graphene is changing the carriers' density by the input voltage. Indeed, by changing the chemical potential, the conductivity of graphene can be controlled. The voltage changes can control the amount of loss and MD [9]. Graphene can conduct plasmonic waves in the terahertz range. As a result, graphene is an excellent choice for terahertz optical devices in the field of surface plasmon polariton [5], [6], [7]. Graphene's layer absorption is one of the most challenging issues in optical modulators. The monolayer of the graphene can absorb 2.3% of the input light, which is reasonable for a single layer of graphene [10], [11].

Furthermore, the monolayer of graphene cannot absorb sufficient light. To address this issue, we increased the number of graphene layers. Anisotropic graphene was utilized and integrated with the h-BN layer for this investigation.

Hexagonal Boron Nitride (h-BN) has attracted much attention due to its unrivaled properties, such as high chemical durability, thermal conductivity, melting temperature, electrical resistance, and 6.5 eV energy gap [12]. The h-BN layers are barrier dielectric layers for optical structures. On the other hand, h-BN layers can modify the graphene band structure [13]. The thickness of the h-BN layer plays a vital role in the modulator's operation. By reducing the h-BN layer's thickness to below 10 nm, it is possible to increase the light confinement [14]. Also, Molybdenum Disulfide (MoS_2), due to its tunable optical emission, the direct energy gap, and the strong plasmon exciton force, which is created between the MoS_2 layers, is one of the critical materials in the recently developed devices [15].

Plasmonic structures are an effective design tool to achieve a customized optoelectronic response [16], [17]. Surface plasmons with light-trapping characteristics at the nanometer range have received much attention in various applications, such as chemical sensing devices, integrated waveguides, and modulators. Surface Plasmons can increase the intensity of the magnetic field [18], [19]. Surface Plasmon Polaritons (SPPs) support both TM and TE modes. SPP occurs at the boundary between metal and dielectric. SPP is a TM wave, and the magnetic field is parallel to the interface [20]. However, both TE and TM can be generated on the surface. Plasmonic structures in the integration of the MoS_2 layer represent extraordinary results [21], [22], [23].

Manuscript received 5 September 2023; revised 2 December 2023; accepted 20 December 2023. Date of publication 25 December 2023; date of current version 15 January 2024. *(Corresponding author: Hamid Vahed.)*

The authors are with the Faculty of Electrical and Computer Engineering, University of Tabriz, Tabriz 5166616471, Iran (e-mail: hosein.karimkhani96@ms.tabrizu.ac.ir; vahed@tabrizu.ac.ir).

Digital Object Identifier 10.1109/JPHOT.2023.3346451

Fast electro-optic modulators are regarded as one of the most important and widely used components in the telecommunications industry and have received considerable attention in recent decades [24], [25]. The most vital characteristics of optical modulators are large bandwidth, high speed, and small footprint [25], [26], [27]. Optical modulators are divided into two major Electro Absorption (EA) modulators and Electro Refractive (ER) modulators categories [28]. ER modulators involve changes in the real part of the effective index through the Pockels effect, while EA modulators are associated with changes in the imaginary part of the effective index through the Franz-Keldysh effect under applied voltage [29], [30]. Electro-absorption modulators can change the Fermi level by applying voltage [31], [32]. The first generation of the modulators was based on the graphene layers with a bandwidth of 1.35 μm to 1.6 μm and 0.1 dB/μm modulation depth [33]. K. Xu et al. proposed a microfiber graphene based modulator with an Al_2O_3 dielectric layer [34]. The modulation bandwidth of this modulator is 82 GHz with 1372 μm active length. B. Wang et al. designed a modulator based on graphene and h-BN layers with 4 dB/μm modulation depth, 2.6 dB/μm loss, and 3.5 FoM [35]. X. Hu et al. demonstrated a graphene based modulator with ultra-thin waveguide [5]. The maximum modulation depth of the investigated modulator was 0.306 dB/μm with 0.0137 dB/μm loss. In recent work, we elaborated a modulator with silver ribbons and h-BN dielectric [36]. The modulation depth was 17.55 dB/μm, and the loss value was 1.47 dB/ μm.

In this study, we proposed a modulator based on graphene and silver ribbons. The results that were investigated are based on simulations and numerical analysis. Here, the loss is one of the challenging points. We aimed to reduce loss while simultaneously increasing the amount of modulation depth. As a result, notable modulation depth was attained in the final structure with four graphene layers. The current structure illustrates how a small-footprint high-speed optical modulator based on the graphene and MoS_2 layers can achieve high modulation depth. This modulator contains silver arrays. These metal arrays can improve the interaction of the input light and graphene. As a result, these structures have excellent light interaction. First, we study the changes in the real and imaginary parts of the effective refractive index regarding chemical potential. Secondly, we calculate modulation depth, FoM, energy consumption, and modulation bandwidth.

II. Modulator Structure and Conductivity of Graphene

A. Structure Properties and Layers Fabrication

The investigated modulators are represented in two different structures. Various structures with various dimensions were studied, and the most efficient structures with high modulation depth rates are illustrated in Fig. 1. Both of the structures consist of SiO_2 substrate, graphene, and h-BN layers. The width of the SiO_2 layer is 1450 nm with a thickness (h) of 300 nm. In the first structure, the h-BN layers with a thickness of 1 nm are placed on the SiO_2 substrate (Fig. 1(a)). The graphene layer is located on the h-BN layer, and at the final step, the MoS_2 layer is posited on the graphene layer, precisely beneath the silver arrays. Silver nanoribbons' thickness (w) and width (b) are 25 nm and 50 nm, respectively. The length of the device is 1450 nm, 1100 nm, 890 nm, and 820 nm, while the g is 50 nm, 25 nm, 10 nm, and 5 nm, respectively. In the second structure, the extra MoS_2, graphene, and h-BN layers are placed on the silver waveguides (Fig. 1(b)). The input beam is shown in Fig. 2; applying a voltage to the Au electrodes changes the graphene's conductivity. Au electrodes serve as the voltage contacts. One of the most crucial issues is the fabrication of various layers. The fabrication parts can be examined with multiple scanning techniques. In the fabrication process of the proposed modulator, h-BN, and graphene layers can be added by the chemical vapor deposition on the SiO_2 wafer substrate. A photoresist mask is placed on the graphene layer to create the Au voltage gate and then removed by a spin-coated process. After the metal evaporation of Au on the structure, the mask is removed by the lift-up process. In the following, the MoS_2 layer is attached to the graphene layer by chemical vapor deposition. Finally, the metal evaporation process is repeated for the second Au voltage gate and Ag grating layers. Fig. 2. represents the 3-D view of the developed structures. The position of the electrodes is shown in Fig. 2, which are placed on top of the graphene layers.

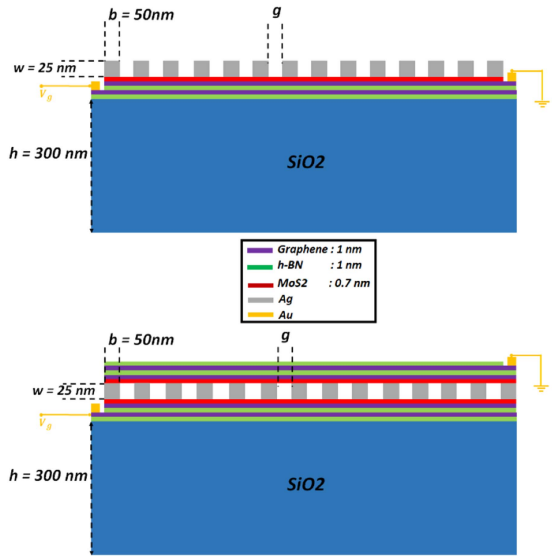

Fig. 1. Cross section view of the (a) first and (b) second proposed optical modulator.

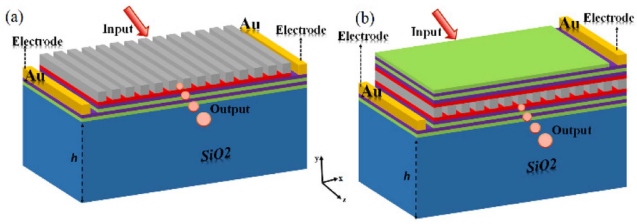

Fig. 2. 3-D view of the (a) first and (b) second proposed modulator.

The thicknesses of the graphene, h-BN, and MoS_2 layers are assumed to be 1 nm, 1 nm, and 0.7 nm, respectively. Then, silver

nanoribbons are fabricated on the structure. The gap between silver nanoribbons is represented with g. The amounts of g are considered in 5 nm, 10 nm, 25 nm, and 50 nm. Finally, the second structure is shown in Fig. 2(b). This study performs in a wavelength range of 1.3 μm to 1.8 μm. The refractive index of h-BN and MoS_2 layers are 1.98 and 4.37, respectively [37], [38].

B. Formulation

Since the graphene electrons have a low density, the Fermi level or chemical potential of the graphene can be tuned by the carrier density [8]. By applying a voltage to the graphene layers, the carriers come together, and the chemical potential can be controlled by voltage [7], [8]. The applied voltage changes the chemical potential of graphene, and these changes in chemical potential can regulate the optical conductivity of graphene. By using the Kubo equation, the relation of the optical conductivity of single-layer graphene can be obtained in both intra-band and inter-band ranges [36], [39], [40]:

$$\begin{aligned}&\sigma(\omega,\mu_c,\tau,T)\\&=\frac{-ie^2}{\pi\hbar^2(\omega-i2\tau)}\left[\int_0^\infty \varepsilon\left(\frac{\partial f_d(\varepsilon)}{\partial\varepsilon}-\frac{\partial f_d(-\varepsilon)}{\partial\varepsilon}\right)d\varepsilon\right]\\&\quad-\frac{ie^2(\omega+i2\tau)}{\pi\hbar^2}\left[\int_0^\infty \frac{f_d(-\varepsilon)-f_d(\varepsilon)}{(\omega+i2\tau)^2-4\left(\frac{\varepsilon}{\hbar}\right)}d\varepsilon\right]\end{aligned}\tag{1}$$

$$\begin{aligned}&\sigma_{intra}(\omega,\mu_c,\tau,T)\\&=\frac{-ie^2K_BT}{\pi\hbar^2(\omega-i\tau^{-1})}\left[\frac{\mu c}{K_BT}+2\ln\left(e^{-\frac{\mu c}{K_BT}}+1\right)\right]\end{aligned}\tag{2}$$

$$\begin{aligned}&\sigma_{inter}(\omega,\mu_c,\tau,T)\\&=\frac{-ie^2}{4\pi\hbar}ln\left(\frac{2|\mu_c|-(\omega-i\tau^{-1})\hbar}{2|\mu_c|+(\omega-i\tau^{-1})\hbar}\right)\end{aligned}\tag{3}$$

Where ω is optical frequency, μ_c is chemical potential, e is the electron charge, $\hbar$ is the reduced Planck constant, T is temperature, K_B is the Boltzmann constant, τ is relaxation time, and $f_d=(1+e^{\frac{\varepsilon-\mu_c}{K_BT}})^{-1}$ is the Fermi Dirac distribution [13]. This study calculated by the finite difference time domain (FDTD) method to investigate the performance of the discussed modulator. The boundary condition is fixed to a perfectly matched layer (PML) with 64 layers to decrease the amount of reflected light. The graphene-based modulators in the THz range are also widespread and have received a lot of attention [9], [36], [41]. The chemical potential of the graphene varies with applied voltage. The applied voltage changes the carrier density of the graphene, and the amount of the μ_c can be calculated from [5], [42]:

$$\mu_c=\hbar\nu_f\sqrt{\pi a_0 V}\tag{4}$$

Where $\nu_f=3\times10^6$ m/s is the Fermi velocity of the electrons in the graphene, $\hbar$ is the reduced Planck constant, $a_0=\frac{\varepsilon_0\varepsilon_r}{de}$ is the capacitor constant, d is the graphene layers thickness, ε_0, and ε_r are the permittivity of vacuum and the relative permittivity of the dielectric [5], [43], and V is the applied voltage. When voltage is applied to the graphene layer, the applied voltage changes the Fermi energy, and finally, the amount of absorption changes.

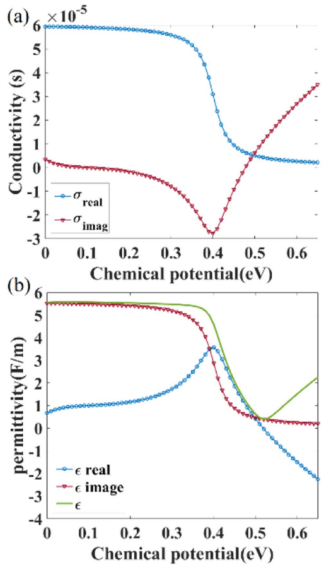

Fig. 3. Real and imaginary part of the graphene's (a) conductivity, (b) permittivity at 1.55 μm wavelength.

The real and imaginary parts of the graphene conductivity at the wavelength of 1.55 μm are depicted in Fig. 3(a). The permittivity of the graphene is calculated as the function of the chemical potential at 1.55 μm in Fig. 3(b). As shown in Fig. 3(b), when the chemical potential increases from 0 eV to 0.65 eV, the permittivity of graphene varies from 0.674+0.565i at 0 eV to −4.195+0.131i at 0.65 eV. When the chemical potential changes from 0.3 eV to 0.5 eV, the imaginary part of the permittivity alters swiftly [44]. The permittivity of graphene at the chemical potential of 0.52 eV is 0. When $\mu_c<0.52$ eV, graphene behaves like a dielectric, and when $\mu_c>0.52$ eV, graphene acts like a metal [36], [43], [44]. As a result, the amount of absorption can be regulated by applying a voltage to the graphene layers.

Generally, when $\mu_c<\hbar\omega/2$, the inter-band transfer and absorption occur, and when $\mu_c>\hbar\omega/2$, the inter-band transfer is blocked, and intra-absorption occurs at very low frequencies [28].

The following important parameter is the modulation depth. The following equation can be used to calculate the modulation depth [43]:

$$MD\ (dB/\mu m)=Loss\ (OFF)-Loss\ (ON).\tag{5}$$

Where Loss(OFF) is the amount of loss at 0 eV and Loss(ON) is the amount of loss at 0.65 eV. The loss value is another momentous parameter of the optical modulators that can be calculated from the following equation [28], [45], [46]:

$$Loss=\frac{10\ Im\left(N_{eff}\right)\ 4\pi}{\lambda_0\ln 10}\tag{6}$$

Where *Im(N_{eff})* is the imaginary part of the refractive index, λ_0 is the free-space wavelength. The amount of the Figure of

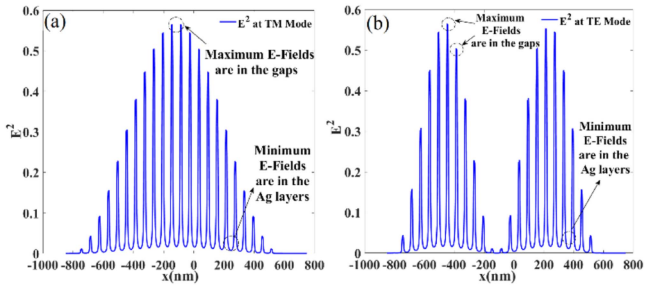

Fig. 4. Electrical field distribution at 1.5 μm for (a) TM and (b) TE mode for the first structure with g = 5 nm at 0.65 eV.

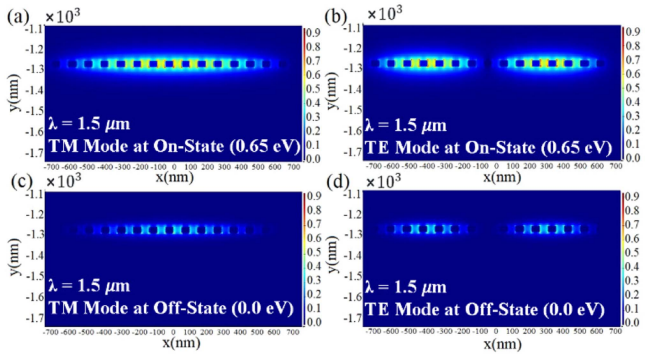

Fig. 5. Electrical field profile at 1.5 μm for (a) TM mode at on-state, (b) TE mode at on-state, (c) TM mode at off-state, and (d) TE mode at off-state for the first structure with g = 5 nm.

Merit (FoM) can be calculated by MD and loss [47], [48]:

$$FoM = \text{MD } (\text{dB}/\mu\text{m}) / \text{PL } (\text{dB}/\mu\text{m}). \tag{7}$$

Where PL is the propagation loss at 0.65 eV chemical potential [47].

III. Results and Discussion

In Fig. 4, TM and TE electric field distributions are demonstrated for the first structure at the wavelength of 1.55 μm with g = 5 nm. According to Fig. 4(a), the field distribution of TM mode is distributed in the middle part of the structure. On the other hand, the TE mode's field distribution is concentrated in two segments of the nanoribbon array (Fig. 4(b)). The mode's field distribution for the second structure is qualitatively similar to the first structure. According to Fig. 4, the maximum field is concentrated between the silver nanoribbon arrays. Also, Fig. 5, depicts the first structure's electrical field profile while the amount of the g is 5 nm. According to Fig. 5(a), while the chemical potential is 0.65 eV, and the modulator operates at the On-State TM mode, an intense electrical field is created between the Ag layers. Also, the electrical field profile for TE mode investigated in Fig. 5. Fig. 5(b) clearly demonstrates that in TE mode, the electrical field is separated into two different parts, and the input light is transmitted in two various paths. Fig. 5(c), (d) depict the electrical field profile for the Off-State. Fig. 5(c), (d) demonstrate that the intensity of the electrical field reduced at 0 eV chemical potential.

The mode overlap in optical devices involving 2D materials ensures that the optical mode supported by the waveguide aligns well with the properties of the 2D material. This alignment is crucial for enhancing light-matter interactions and optimizing the device's performance. Mode overlap refers to the spatial alignment or correspondence between the optical mode supported by the waveguide and the optical properties of the 2D material. This concept is particularly relevant in devices such as modulators, detectors, and light emitters that leverage the unique properties of 2D materials to control or manipulate light at the nanoscale. Designing optical devices with optimal mode overlap often involves careful engineering of the device's geometry, dimensions, and the properties of the integrated 2D material.

Maximizing mode overlap can enhance the efficiency and functionality of the device. Achieving a strong mode overlap is crucial for optimizing the device's interaction between light and 2D materials. It can enhance light-matter interactions, such as absorption or emission processes, and influence the device's overall performance. In this section, the loss and the real part of the effective index changes ($Re(N_{eff})$) in terms of the chemical potential for different values of g are investigated at the wavelength of 1.55 μm. Fig. 6(a)–(c), shows the loss as a function of the chemical potential from 0 eV to 0.65 eV for both structures with different values of the g parameter.

It can be seen that, in both structures, the loss has increased when the amount of the g decreases from 50 nm to 5 nm. Accordingly, when the chemical potential increases from 0 eV (Off-State) to 0.65 eV (On-State), the loss decreases, and this reduction occurred at 0.4 eV, 0.35 eV, and 0.3 eV chemical potentials at the wavelengths of 1.3 μm, 1.55 μm, and 1.8 μm. This sudden reduction in the loss amount is expected because of the permittivity changes.

Fig. 6(a)–(c) illustrates that the structures with the lower amount of the g have an exorbitant slope. The amount of the loss decreases to lower rates when the chemical potential is 0.4 eV, 0.35 eV, and 0.3 eV for the wavelengths of 1.3 μm, 1.55 μm, and 1.8 μm. While the chemical potential is lower than 0.4 eV, 0.35 eV, and 0.3 eV for the wavelengths of 1.3 μm, 1.55 μm, and 1.8 μm the modulator operates at the high loss region, however, when the chemical potential is higher than 0.4 eV, 0.35 eV, and 0.3 eV for the wavelengths of 1.3 μm, 1.55 μm, and 1.8 μm, the proposed modulator operates at the low loss region.

Fig. 7(a)–(c) shows the $Re(N_{eff})$ as a function of the chemical potential from 0 eV to 0.65 eV. According to Fig. 7(a)–(c), when the amount of g decreases from 50 nm to 5 nm, the amount of $Re(N_{eff})$ enhances. Accordingly, when the chemical potential increases from 0 eV to 0.65 eV, refractive indices have decreased. This reduction has occurred at the chemical potential of 0.4 eV when the wavelength is 1.3 μm. While, the chemical potential is 0.3 eV for the wavelengths of 1.5 μm, and 1.8 μm, this reduction has occurred. Fig. 7(a)–(c) demonstrates that, the highest amount of the refractive index relates to the second structure with g = 5 nm. Also, according to Fig. 7(a)–(c), for different wavelengths, the amount of the changes in the refractive index between 0 eV and 0.65 eV are extremely small.

In the following, the amount of loss and $Re(N_{eff})$ changes in the verses of wavelength are depicted in Figs. 8 and 9. The

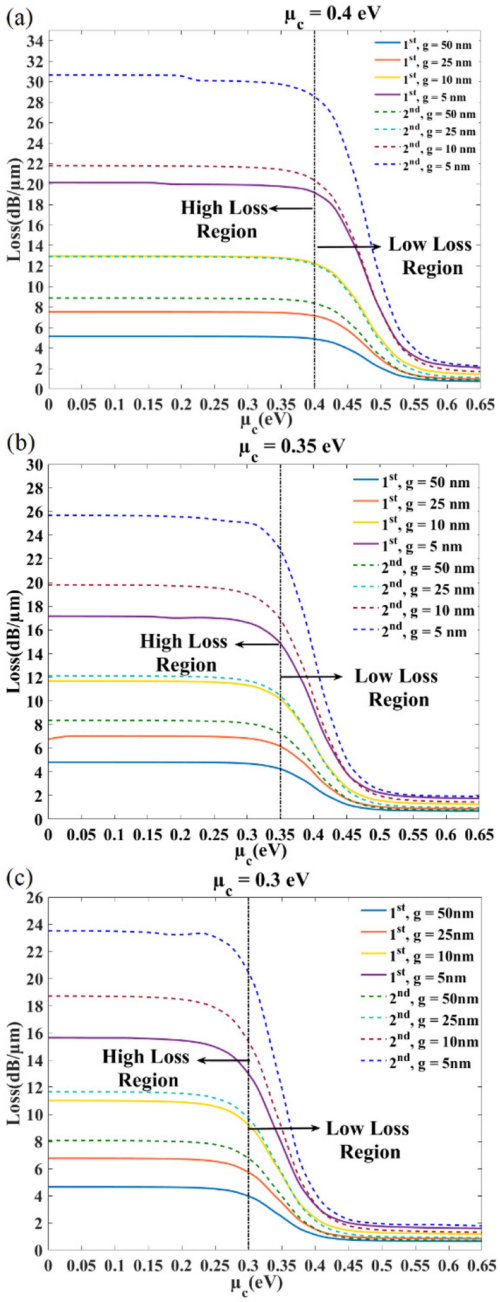

Fig. 6. Loss as a function of μ_c for both of the structures at (a) wavelength of 1.3 μm, (b) wavelength of 1.55 μm, and (c) wavelength of 1.8 μm.

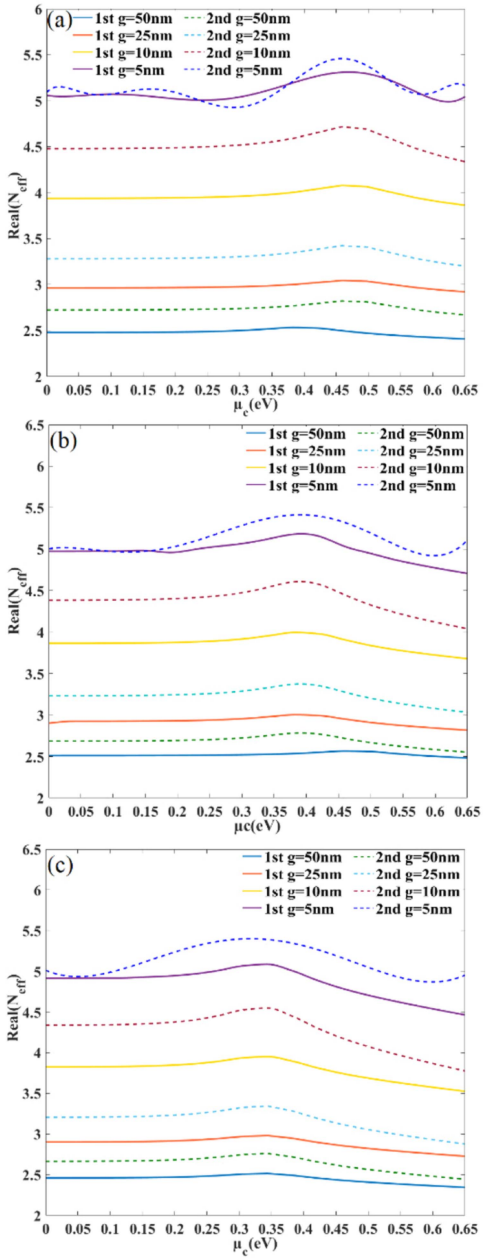

Fig. 7. $Re(N_{eff})$ as a function of chemical potential for both of the structures at wavelength of (a) 1.3 μm, (b) 1.55 μm, and (c) 1.8 μm.

amount of the changes is shown for On-State and Off-State in two structures with g = 5 nm (Figs. 8 and 9).

According to Fig. 8, by increasing the wavelength, the amount of loss decreases in both 0 eV and 0.65 eV chemical potentials. At the chemical potential of 0 eV, the amount of loss is 20.12 dB/μm at 1.3 μm in the first structure, and finally, at the wavelength of 1.5 μm, the amount of the loss is 17 dB/μm. In the second structure, at the chemical potential of 0 eV, the loss is 30.6 dB/μm, and finally, at the wavelength of 1.5 μm, the loss is 25 dB/μm.

According to Fig. 9, it is clear, in both of the chemical potentials, with increasing the wavelength from 1.3 μm to 1.8 μm, the $Re(N_{eff})$ decreases. Moreover, by increasing the chemical potential from 0 eV to 0.65 eV, the value of the $Re(N_{eff})$ has been reduced. In both of the chemical potentials, the $Re(N_{eff})$ has an identical pattern. Furthermore, the amount of change at 0.65 eV is greater than 0 eV, and the changes have a steep slope.

The modulation depth (MD) in terms of the wavelength was calculated for both structures in Fig. 10(a), in both structures, the modulation depth decreased when the g value was raised. In the first structure, at g = 5 nm, the MD of 15.2 dB/μm is obtained at the wavelength of 1.55 μm. For the second structure with g = 5 nm, the MD is 23.37 dB/μm at the wavelength of 1.55 μm. The highest amount of the MD is 18.03 dB/μm for the first structure and 28.37 dB/μm for the second structure, which is

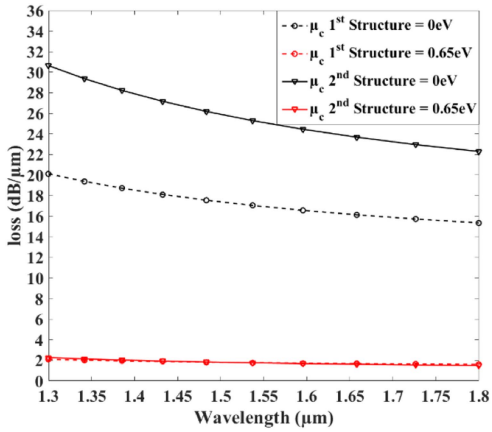

Fig. 8. Loss as a function of wavelength for two values of chemical potential 0.0 eV and 0.65 eV with g = 5 nm for the first and the second structure.

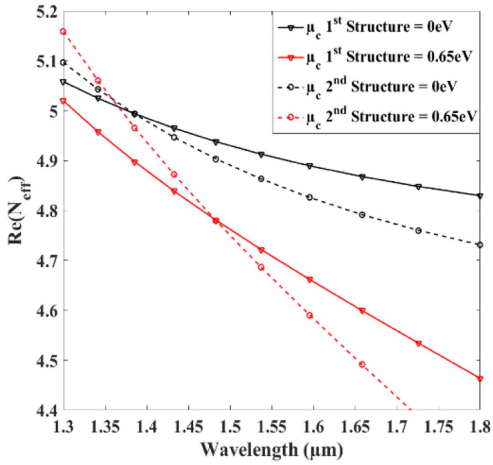

Fig. 9. $Re(N_{eff})$ as a function of wavelength for chemical potential of 0.0 eV and 0.65 eV with g = 5 nm for the first and the second structure.

related to 1.3 μm wavelength. The amount of the MD in the first simulation is 4.37 dB/μm, and in the last simulation, it increased six fold.

Secondly, FoM is plotted in Fig. 10(b) for both of the structures. In the proposed structures, with increasing the amount of the g, the FoM decreased. In the first structure, at g = 5 nm, the FoM of 16.05 is achieved at the wavelength of 1.55 μm. For the second structure with g = 5 nm, the amount of the FoM is 37.11 at the wavelength of 1.55 μm. The highest amount of the FoM is 62.93, which is related to the second structure with g = 5 nm. Additionally, the amount of the modulation depth can be changed with the amount of the g gap.

In the following, the amount of the MD as a function of g (gap) is illustrated in Fig. 11(a). Finally, the amount of the and the gate voltage as a function of the chemical potential is represented in Fig. 11(b). In this study, the On-State and the Off-State voltage are 2.37 V and 0 V, respectively.

Extinction ratio (ER) is one of the most essential and critical parameters in electro-optical modulators. Extinction ratio can be calculated by (8), which shows that the ER is entirely dependent

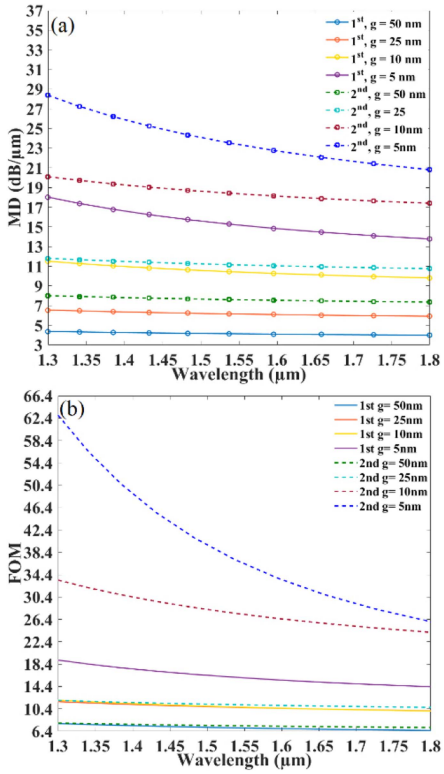

Fig. 10. (a) MD as function of wavelength with different values of g for the first and the second structures, (b) FoM as function of wavelength for different values of g for the first and the second structures.

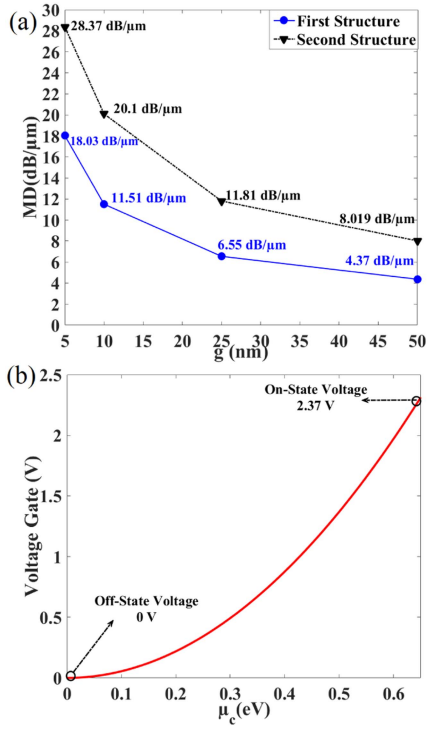

Fig. 11. (a) Dependence of modulation depth to the g at 1.3 μm, (b) Gate voltage changes in terms of the chemical potential.

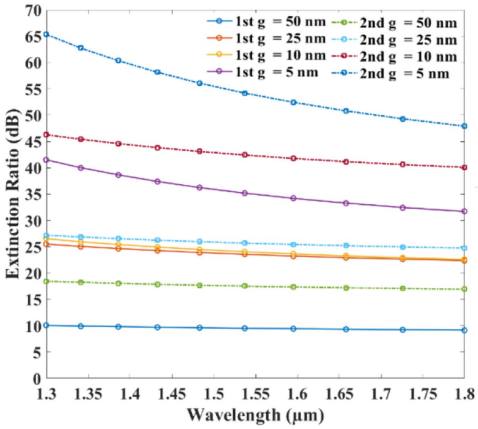

Fig. 12. ER as function of wavelength with different values of g for the first and the second structures.

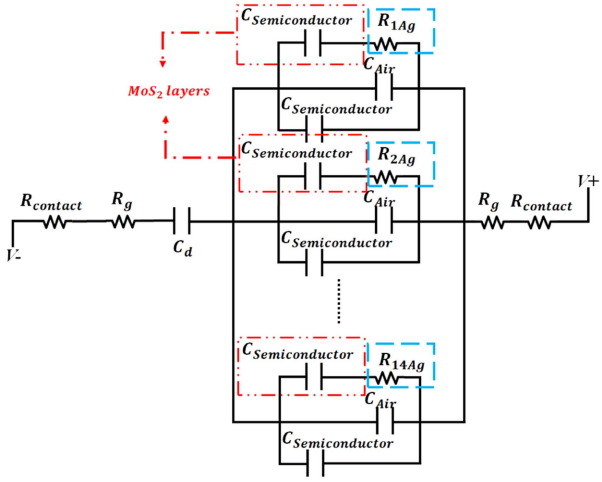

Fig. 13. Equivalent circuit of the proposed modulator.

on the modulator's output power in both the On-State and Off-State. Fig. 12. depicts the ER variations in the wavelength range of 1.3 μm to 1.8 μm [49], [50].

$$ER\,(dB) = 10\,[(\log_{10} P_{On\ State}) - (\log_{10} P_{Off\ State})] \quad (8)$$

Fig. 12. shows that when the wavelength increases from 1.3 μm to 1.8 μm, the ER drops. ER, on the other hand, rises when the gap between Ag layers' narrows. The maximum ER is 65.34 dB at 1.3 μm and is related to the second structure with a 5 nm gap. Finally, for further investigation, we discuss other substantial parameters in modulators. In optical modulators, the footprint, the energy per bit (E_{bit}), and the modulation bandwidth (f_{3dB}) play an essential role. These parameters are crucial and valuable factors in the selection of modulators. The amount of the (f_{3dB}) can be calculated by [43], [49], [51]:

$$f_{3dB} = 1/2\pi RC \quad (9)$$

Where the capacitance is $C = \varepsilon_0\,\varepsilon_r S/d$, ε_0 is the permittivity of the vacuum, and ε_r is the permittivity of h-BN, S is the area, and d is the thickness of h-BN layer, respectively [52]. The amount of C is 11.20 fF. and R is the series resistance of the device, which is assumed 33 Ω [53], and the equivalent circuit of the proposed modulator is depicted in Fig. 13. Then E_{bit} is calculated by (10) [36], [43], [54].

$$E_{bit} = C\Delta V^2/4 \quad (10)$$

Where C is the capacitance and ΔV is the voltage between On-State and Off-State [36], [43]. According to (4), the amount of the ΔV can be calculated by (11) [55]:

$$\Delta V = V_{gate-On\ state} - V_{gate-Off\ state} = \mu_c^2\, dq/\hbar^2 \nu_F^2 \varepsilon_0 \varepsilon_r \quad (11)$$

Fig. 11(b) represents the ΔV changes in terms of the chemical potential.

As can be seen in Fig. 13, $R_{contact}$ and R_g are related to the gate resistance and the graphene layers resistance, respectively. R_{nAg} and n are the silver array's resistance and the number of the array. $C_{Semiconductor}$ is the capacitance of the MoS_2 layers. C_{Air} is the capacitance of the air between the silver layers, and C_d is the dielectric layer's capacitance.

V. Conclusion

In this work, we investigated an EA optical modulator based on graphene and h-BN layers placed around silver nanoribbon arrays. We analyzed the MD and the FoM in this modulator and not only achieved high modulation depth but also attempted to attain a low loss. In detail, both of the structures have a high modulation depth. The proposed structure reached MD and FoM as high as 28.37 dB/μm and 62.93, respectively. Furthermore, modulation bandwidths as high as 411.25 GHz and low E_{bit} in these structures have been investigated. The numerical simulation denotes that this modulator can achieve high MD with a small footprint and low energy consumption. The investigated ER is 65.34 dB, while the amount of the switching voltage is 2.37 V. Also, the amount of the loss and real part of the refractive index for the proposed structure is 2.2 dB/μm and 5.65 dB/μm, respectively.

References

[1] K. S. Novoselov et al., "Electric field effect in atomically thin carbon films," *Science*, vol. 306, no. 5696, pp. 666–669, 2004.
[2] K. S. Novoselov et al., "Two-dimensional gas of massless Dirac fermions in graphene," *Nature*, vol. 438, no. 7065, 2005, Art. no. 197.
[3] A. H. C. Neto, F. Guinea, N. M. R. Peres, K. S. Novoselov, and A. K. Geim, "The electronic properties of graphene," *Rev. Mod. Phys.*, vol. 81, no. 1, pp. 197–200, 2009.
[4] S. Edelstein, S. R. K. C. Indukuri, N. Mazurski, and U. Levy, "Waveguide-integrated mid-IR photodetector and all-optical modulator based on inter-layer excitons absorption in a WS2/HfS2 heterostructure," *Nanophotonics*, vol. 11, no. 19, pp. 4337–4345, 2022.
[5] X. Hu, Y. Zhang, D. Chen, X. Xiao, and S. Yu, "Design and modeling of high efficiency graphene intensity/phase modulator based on ultra-thin silicon strip waveguide," *J. Lightw. Technol.*, vol. 37, no. 10, pp. 2284–2292, May 2019.
[6] D. S. Jessop et al., "Graphene based plasmonic terahertz amplitude modulator operating above 100 MHz," *Appl. Phys. Lett.*, vol. 108, no. 17, 2016, Art. no. 171101.
[7] X. Hu and J. Wang, "High figure of merit graphene modulator based on long-range hybrid plasmonic slot waveguide," *IEEE J. Quantum Electron.*, vol. 53, no. 3, Jun. 2017, Art. no. 7200308.
[8] Y. Meng et al., "Waveguide engineering of graphene optoelectronics—Modulators and polarizers," *IEEE Photon. J*, vol. 10, no. 1, Feb. 2018, Art. no. 6600217.

[9] B. Xiao et al., "A terahertz modulator based on graphene plasmonic waveguide," *IEEE Photon. Technol. Lett.*, vol. 27, no. 20, pp. 2190–2192, Oct. 2015.

[10] B. Zhao, J. M. Zhao, and Z. M. Zhang, "Enhancement of near-infrared absorption in graphene with metal gratings," *Appl. Phys. Lett.*, vol. 105, no. 3, 2014, Art. no. 31905.

[11] Y. Xu et al., "High sensitivity ultraviolet graphene-metamaterial integrated electro-optic modulator enhanced by superlubricity," *Nanophotonics*, vol. 11, no. 16, pp. 3547–3557, 2022.

[12] H. X. Jiang and J. Y. Lin, "Hexagonal boron nitride for deep ultraviolet photonic devices," *Semicond. Sci. Technol.*, vol. 29, no. 8, 2014, Art. no. 084003.

[13] G. W. Hanson, "Dyadic Green's functions and guided surface waves for a surface conductivity model of graphene," *J. Appl. Phys.*, vol. 103, no. 6, 2008, Art. no. 064302.

[14] Q. Zhang, Z. Zhen, C. Liu, D. Jariwala, and X. Cui, "Gate-tunable polariton superlens in 2D/3D heterostructures," *Opt. Exp.*, vol. 27, no. 13, pp. 18628–18641, 2019.

[15] B. Li et al., "Single-nanoparticle plasmonic electro-optic modulator based on MoS_2 monolayers," *ACS Nano*, vol. 11, no. 10, pp. 9720–9727, 2017.

[16] F. Della Picca et al., "Tailored hypersound generation in single plasmonic nanoantennas," *Nano Lett.*, vol. 16, no. 2, pp. 1428–1434, 2016.

[17] H. Karimkhani, A. Attariabad, and H. Vahed, "High sensitive plasmonic sensor with simple design of the ring and the disk resonators," *Opt. Quantum Electron.*, vol. 54, no. 6, pp. 1–13, 2022.

[18] W. L. Barnes, A. Dereux, and T. W. Ebbesen, "Surface plasmon subwavelength optics," *Nature*, vol. 424, no. 6950, pp. 824–830, 2003.

[19] S. Kim, J. Jin, Y.-J. Kim, I.-Y. Park, Y. Kim, and S.-W. Kim, "High-harmonic generation by resonant plasmon field enhancement," *Nature*, vol. 453, no. 7196, pp. 757–760, 2008.

[20] M. Heidari and V. Ahmadi, "Graphene-based mid-infrared plasmonic isolator with multimode interferometer," *Opt. Lett.*, vol. 45, no. 20, pp. 5764–5767, 2020.

[21] Z. Li et al., "Active light control of the MoS_2 monolayer exciton binding energy," *ACS Nano*, vol. 9, no. 10, pp. 10158–10164, 2015.

[22] Y. Kang et al., "Plasmonic hot electron induced structural phase transition in a MoS_2 monolayer," *Adv. Mater.*, vol. 26, no. 37, pp. 6467–6471, 2014.

[23] T. Hong, B. Chamlagain, S. Hu, S. M. Weiss, Z. Zhou, and Y.-Q. Xu, "Plasmonic hot electron induced photocurrent response at MoS_2–metal junctions," *ACS Nano*, vol. 9, no. 5, pp. 5357–5363, 2015.

[24] K. Kim, J.-Y. Choi, T. Kim, S.-H. Cho, and H.-J. Chung, "A role for graphene in silicon-based semiconductor devices," *Nature*, vol. 479, no. 7373, pp. 338–344, 2011.

[25] E. Heidari et al., "Integrated ultra-high-performance graphene optical modulator," *Nanophotonics*, vol. 11, pp. 4011–4016, 2022.

[26] D. A. B. Miller, "Device requirements for optical interconnects to silicon chips," *Proc. IEEE*, vol. 97, no. 7, pp. 1166–1185, Jul. 2009.

[27] M. Kauranen and A. V. Zayats, "Nonlinear plasmonics," *Nature Photon.*, vol. 6, no. 11, pp. 737–748, 2012.

[28] A. Al Sayem, M. R. C. Mahdy, I. Jahangir, and M. S. Rahman, "Ultrathin ultra-broadband electro-absorption modulator based on few-layer graphene based anisotropic metamaterial," *Opt. Commun.*, vol. 384, pp. 50–58, 2017.

[29] R. Amin, R. Maiti, J. B. Khurgin, and V. J. Sorger, "Performance analysis of integrated electro-optic phase modulators based on emerging materials," *IEEE J. Sel. Topics Quantum Electron.*, vol. 27, no. 3, May/Jun. 2021, Art. no. 3300211.

[30] J. Wang, X. Zhang, Y. Chen, Y. Geng, Y. Du, and X. Li, "Design of a graphene-based silicon nitride multimode waveguide-integrated electro-optic modulator," *Opt. Commun.*, vol. 481, 2021, Art. no. 126531.

[31] M. A. Sharif, B. Ghafary, and M. H. M. Ara, "A novel graphene-based electro-optical modulator using modulation instability," *IEEE Photon. Technol. Lett.*, vol. 28, no. 24, pp. 2897–2900, Dec. 2016.

[32] H. Allahverdizade, S. Aghdasinia, H. Younesiraad, and M. Bemani, "A theoretical approach to zero-reflection toroidal curved metasurfaces," *Sci. Rep.*, vol. 13, no. 1, 2023, Art. no. 6682.

[33] M. Liu et al., "A graphene-based broadband optical modulator," *Nature*, vol. 474, no. 7349, pp. 64–67, 2011.

[34] K. Xu et al., "High-speed traveling-wave modulator based on graphene and microfiber," *J. Lightw. Technol.*, vol. 36, no. 20, pp. 4730–4735, Oct. 2018.

[35] B. Wang, S. Blaize, J. Seok, S. Kim, H. Yang, and R. Salas-Montiel, "Plasmonic-based subwavelength graphene-on-hBN modulator on silicon photonics," *IEEE J. Sel. Topics Quantum Electron.*, vol. 25, no. 3, May/Jun. 2019, Art. no. 4600706.

[36] H. Karimkhani and H. Vahed, "Hybrid broadband optical modulator based on multi-layer graphene structure and silver nanoribbons," *Opt. Quantum Electron.*, vol. 52, no. 5, 2020, Art. no. 229, doi: 10.1007/s11082-020-02354-0.

[37] M. S. Ullah, A. H. Bin Yousuf, A. D. Es-Sakhi, and M. H. Chowdhury, "Analysis of optical and electronic properties of MoS_2 for optoelectronics and FET applications," *AIP Conf. Proc.*, vol. 1957, no. 1, 2018, Art. no. 020001.

[38] H. Karimkhani and H. Vahed, "An optical modulator with ridge-type silicon waveguide based on graphene and MoS_2 layers and improved modulation depth," *Opt. Quantum Electron.*, vol. 53, no. 5, pp. 1–10, 2021.

[39] X. He, F. Liu, F. Lin, and W. Shi, "Investigation of terahertz all-dielectric metamaterials," *Opt. Exp.*, vol. 27, no. 10, pp. 13831–13844, 2019.

[40] H. Li, W. Xu, Q. Cui, Y. Wang, and J. Yu, "Theoretical design of a reconfigurable broadband integrated metamaterial terahertz device," *Opt. Exp.*, vol. 28, no. 26, pp. 40060–40074, 2020.

[41] A. Singh, M. Andrello, N. Thawdar, and J. M. Jornet, "Design and operation of a graphene-based plasmonic nano-antenna array for communication in the terahertz band," *IEEE J. Sel. Areas Commun.*, vol. 38, no. 9, pp. 2104–2117, Sep. 2020.

[42] D. Zeng, S. Zong, G. Liu, W. Yuan, X. Liu, and Z. Liu, "Dynamically electrical/thermal-tunable perfect absorber for a high-performance terahertz modulation," *Opt. Exp.*, vol. 30, no. 22, pp. 39736–39746, 2022.

[43] L. Ye, K. Sui, Y. Zhang, and Q. H. Liu, "Broadband optical waveguide modulators based on strongly coupled hybrid graphene and metal nanoribbons for near-infrared applications," *Nanoscale*, vol. 11, no. 7, pp. 3229–3239, 2019.

[44] T. Lian et al., "Electro-absorption optical modulator based on graphene-buried polymer waveguides," *IEEE Photon. J.*, vol. 12, no. 4, Aug. 2020, Art. no. 6601610.

[45] S. Qu, C. Ma, and H. Liu, "Tunable graphene-based hybrid plasmonic modulators for subwavelength confinement," *Sci. Rep.*, vol. 7, no. 1, pp. 1–8, 2017.

[46] Y. Gui et al., "100 GHz micrometer-compact broadband monolithic ITO Mach–Zehnder interferometer modulator enabling 3500 times higher packing density," *Nanophotonics*, vol. 11, pp. 4001–4009, 2022.

[47] Y. Zhu et al., "Hybrid plasmonic graphene modulator with buried silicon waveguide," *Opt. Commun.*, vol. 456, 2020, Art. no. 124559.

[48] H. Karimkhani and H. Vahed, "A broadband optical modulator based on rib-type silicon waveguide including graphene and h-BN layers," *Optik (Stuttg)*, vol. 254, 2022, Art. no. 168633.

[49] H. Karimkhani and H. Vahed, "A structure of electro-absorption hybrid plasmonic modulator using silver nano-ribbon," *Opt. Quantum Electron.*, vol. 55, no. 10, 2023, Art. no. 894, doi: 10.1007/s11082-023-05177-x.

[50] J.-S. Kim and J. T. Kim, "Silicon electro-optic modulator based on an ITO-integrated tunable directional coupler," *J. Phys. D. Appl. Phys.*, vol. 49, no. 7, 2016, Art. no. 075101.

[51] T. Lian et al., "Mode-selective modulator and switch based on graphene-polymer hybrid waveguides," *Opt. Exp.*, vol. 30, no. 13, pp. 23746–23755, 2022.

[52] N. Dhingra, H. Mehrvar, and P. Berini, "High-speed polarization-independent plasmonic modulator on a silicon waveguide," *Opt. Exp.*, vol. 31, no. 14, pp. 22481–22496, 2023.

[53] H. Vahed and S. S. Ahmadi, "Graphene-based plasmonic electro-optic modulator with sub-wavelength thickness and improved modulation depth," *Appl. Phys. B*, vol. 123, no. 11, 2017, Art. no. 265.

[54] H. Zeng, J. Fan, Y. Zhang, Y. Su, C. Qiu, and W. Gao, "Graphene plasmonic spatial light modulator for reconfigurable diffractive optical neural networks," *Opt. Exp.*, vol. 30, no. 8, pp. 12712–12721, 2022.

[55] S. Tavana, S. Bahadori-Haghighi, and M. H. Sheikhi, "High-performance electro-optical switch using an anisotropic graphene-based one-dimensional photonic crystal," *Opt. Exp.*, vol. 30, no. 6, pp. 9269–9283, 2022.